SyntEyes: A Higher-Order Statistical Eye Model for Healthy Eyes

Jos J. Rozema,[1,2] Pablo Rodriguez,[3] Rafael Navarro,[3] and Marie-José Tassignon[1,2]

[1]Department of Ophthalmology, Antwerp University Hospital, Edegem, Belgium
[2]Department of Medicine and Health Sciences, Antwerp University, Wilrijk, Belgium
[3]Instituto de Ciencia de Materiales de Aragón, Consejo Superior de Investigaciones Científicas and Universidad de Zaragoza, Facultad de Ciencias, Zaragoza, Spain

Correspondence: Jos J. Rozema, Department of Ophthalmology, Antwerp University Hospital, Wilrijkstraat 10, 2650 Edegem, Belgium; Jos.Rozema@uza.be.

Submitted: August 28, 2015
Accepted: December 24, 2015

Citation: Rozema JJ, Rodriguez P, Navarro R, Tassignon M-J. SyntEyes: a higher order statistical eye model for healthy eyes. *Invest Ophthalmol Vis Sci*. 2016;57:683–691. DOI:10.1167/iovs.15-18067

Purpose. Stochastic eye models are a method to generate random biometry data with the variability found in the general population for use in optical calculations. This work improves the accuracy of a previous model by including the higher-order shape parameters of the cornea.

Methods. The right eye biometry of 312 subjects (40.8 ± 11.0 years of age) were measured with an autorefractometer, a Scheimpflug camera, an optical biometer, and a ray tracing aberrometer. The corneal shape parameters, exported as Zernike coefficients, were converted to eigenvectors for dimensional reduction. The remaining 18 parameters were modeled as a sum of two multivariate Gaussians, from which an unlimited number of synthetic data sets (SyntEyes) were generated. After conversion back to Zernike coefficients, the data were introduced into ray tracing software.

Results. The mean values of nearly all SyntEyes parameters were statistically equal to those of the original data (two one-sided *t*-test, $P > 0.05/109$, Bonferroni correction). The variability of the SyntEyes parameters was similar to the original data for most important shape parameters and intraocular distances (*F*-test, $P < 0.05/109$), but significantly lower for the higher-order shape parameters (*F*-test, $P > 0.05/109$). The same was seen for the correlations between higher-order shape parameters. After applying simulated cataract or refractive surgery to the SyntEyes model, a very close resemblance to previously published clinical outcome data was seen.

Conclusions. The SyntEyes model produces synthetic biometry that closely resembles clinically measured data, including the normal biological variations in the general population.

Keywords: statistical eye model, ocular biometry

When making any kind of refractive calculations in physiological optics, it is essential to start from a realistic set of biometric dimensions and curvatures that represent the optical structure of the eye. In a clinical setting, most of these parameters are readily available through standard biometric methods, such as Scheimpflug tomography and partial coherence interferometry. Many non–hospital-affiliated researchers, however, have only limited access to real biometry data, which compels them to use eye models instead. These models represent a fixed, nearly emmetropic biometry set based on a population average, such as the works of Gullstrand,[1] Navarro and colleagues,[2,3] and Liou and Brennan,[4] that have played an essential role in many great scientific developments of the last century. However, despite these contributions, such generic eye models do not take the wide variety in ocular biometry into account that was observed in epidemiologic biometry studies. For example, assuming a tolerance of ±0.25 diopters (D) in keratometry and ±0.10 mm in axial length, the Gullstrand eye model would correspond with only 0.51% of the 1178 Western European eyes in our previous work on the epidemiology of ocular biometry.[5] Similarly, the more recent Navarro and Liou and Brennan models both correspond with 1.02% of the same cohort. To study eyes that deviate from these average values, these generic models are often customized, for example, by inserting measured biometry values into a chosen eye model while keeping other unmeasured (or unmeasurable) values unaltered.[6–8] Alternatively, customization can also be achieved by considering the unmeasured parameters as free variables in an optimization process until, for example, the ocular wavefront of the individual eye model matches the measured values.[9,10] Although this approach leads to a data set much closer to the patient's actual biometry, one has to make sure that the inserted biometry parameters are very complete to avoid introducing systematic errors resulting from a lack of correlation between the measured data and the unaltered parameters of the original eye model. Moreover, access to measured data is still required for customized modeling.

Another approach is to use stochastic modeling, which produces an unlimited amount of synthetic biometry data sets (SyntEyes) that has statistical properties identical to that of the original data it is based on. Apart from the initial data needed to define the model, this concept requires no biometry measurements from the end user, making it an interesting tool for vision scientists, as well as for simulating clinical procedures. This statistical eye model was developed by our team several years ago,[11] based on ideas proposed earlier by Sorsby et al.,[12] Thibos

This work is licensed under a Creative Commons Attribution-NonCommercial-NoDerivatives 4.0 International License.

Downloaded From: http://iovs.arvojournals.org/pdfaccess.ashx?url=/data/Journals/IOVS/934916/ on 05/17/2016

Table 1. Overview of the Parameters Used

Parameter	Unit	Determined by	Description
SE	D	Autorefractometer	Spherical equivalent refraction at spectacle plane
J_0, J_{45}	D	Autorefractometer	Jackson cylinders at spectacle plane
Z_n^m (*WF*)	μm	iTrace	Zernike coefficient of ocular wavefront
Z_n^m (*CA*)	mm	Pentacam	Zernike coefficient of anterior corneal surface elevation
Z_n^m (*CP*)	mm	Pentacam	Zernike coefficient of posterior corneal surface elevation
CCT	μm	Pentacam	Central corneal thickness
EC_i	μm	Reference 15	Eigencornea
ACD	mm	Pentacam	Anterior chamber depth (corneal epithelium to lens)
T	mm	Lenstar	Lens thickness
L	mm	Lenstar + 0.200 mm	Axial length (including 0.2-mm retinal thickness)
RT	mm	0.200	Thickness of retinal layers
V	mm	$L - CCT - ACD - T - RT$	Vitreous depth
P_L	D	Reference 17	Lens power using Bennett method
r_{La}	mm	Reference 16	Anterior radius of curvature of lens
r_{Lp}	mm	Reference 16	Posterior radius of curvature of lens
Z_n^m (*int*)	mm	Calibration	Zernike coefficient of internal refractive components
LTx, LT_y	°	–	Lens tilt
LSx, LS_y	mm	–	Lens shift
n_c	–	1.376	Refractive index of cornea
n	–	1.336	Refractive index of aqueous and vitreous humors
n_L	–	Reference 16	Refractive index of crystalline lens

et al.,[13] and Zhao.[14] However, although this model successfully reproduced the distributions of the ocular biometry in West European subjects, it was restricted to producing only lower orders of wavefront aberrations, thus limiting its applications.

The purpose of the current work is therefore to improve the accuracy of the earlier model by including a Zernike description of the corneal shape. Furthermore, a number of technical improvements will be introduced to enhance its performance, such as principal component analysis to reduce the number of parameters,[15] more accurate methods to estimate the crystalline lens shape[16] and power,[17] and a linear combination of multivariate Gaussians[5] instead of refractive filtering. After verification of the model, examples will be given of possible applications.

Methods

Subjects and Measurements

The biometric data were taken from 312 healthy right eyes of 312 Western European Caucasian subjects recruited from the personnel of the Antwerp University Hospital and people of the nearby suburban area of Edegem for the purpose of this study. The cohort consisted of 42.9% men and 57.1% women, with an average age of 40.8 ± 11.0 years (range, 20.2–59.6 years). Exclusion criteria were prior ocular pathology or surgery, an intraocular pressure higher than 22 mm Hg, and wearing rigid gas permeable (RGP) contact lenses less than 1 month before testing. Subjects were not dilated for their investigations, which could have had some minor influence on the biometric readings in younger subjects.

For all subjects, the shape and dimensions of the cornea and anterior chamber were determined using a Scheimpflug camera (Oculus Pentacam, Wetzlar, Germany), lens thickness *T* and axial length *L* were measured with a noncontact optical biometer (Haag-Streit Lenstar, Koenitz, Switserland), and the ocular wavefront was determined using a ray tracing aberrometer (Tracey iTrace, Houston, TX, USA). Furthermore, the refraction was determined using an autorefractometer (Nidek ARK 700, Nidek, Gamagori, Japan) and the intraocular pressure with a pneumotonometer (Reichert ORA, Depew, NY, USA). A detailed overview of the parameters used in the modeling is given in Table 1.

Modeling of the Eye

The present model is loosely based on the Navarro eye model,[2] from which the basic structure and some of the clinically inaccessible parameters are taken. It comprises two Zernike surfaces representing the cornea, two aspherical surfaces representing the crystalline lens, a stop at the pupil plane, and a spherical retina (Table 2). The anterior lens surface also contains an additional Zernike phase correction to account for wavefront aberrations of noncorneal origins, such as the intrinsic aberrations of the crystalline lens and those resulting from the lenticular alignment relative to the cornea.

Cornea. Both the anterior and posterior corneal surfaces are represented by means of eighth-order Zernike polynomials (45 parameters) with a diameter of 6.50 mm. Together with the central corneal thickness CCT, this forms a complete description of the corneal shape. As the large number of parameters involved could cause dimensionality problems during the Gaussian modeling, we used principal component analysis to compress the number of dimensions from 91 corneal parameters to 12 eigenvectors (eigencorneas [ECs]) while retaining 99.5% of the original variability.[15] The remaining 0.5% of variability lies mostly in the higher-order aberrations and is of no real consequence to the model (Supplementary Material A). These eigencorneas are used during the stochastic process and converted back to Zernike coefficients and CCT afterward.

Crystalline Lens. As most lens parameters are not yet measurable by means of routine clinical equipment, alternative methods have to be used to obtain realistic estimations. The lens power P_L is calculated from the ocular biometry using the Bennett equation with optimized parameters,[17,18] and the lens radii r_{La} and r_{lp} are derived from regressions based on lens power P_L and lens thickness *T*.[16] Similarly, a regression was used to estimate missing lens thickness values in eyes where it is missing.[16] Once lens power and radii are available, the equivalent refractive index of the lens may be derived using equation 3 in Reference 16. Finally, the asphericity of both lens surfaces is taken from the Navarro model.[2]

Investigative Ophthalmology & Visual Science

Downloaded From: http://iovs.arvojournals.org/pdfaccess.ashx?url=/data/Journals/IOVS/934916/ on 05/17/2016

Table 2. List of Parameter Values Used in the Eye Model

	Cornea			Crystalline Lens		
Parameter	**Anterior**	**Posterior**	**Pupil**	**Anterior**	**Posterior**	**Retina**
Surface type	Zernike	Zernike	Spherical	Aspherical + Zernike*	Aspherical	Spherical
Diameter, mm	6.50	6.50	5.00	5.50	5.50	6.00
Radius, mm	EC	EC	∞	r_{La}	r_{Lp}	−12.00
Asphericity	EC	EC	–	−3.1316	−1	–
Thickness	EC	ACD	–	T	V	–
Refractive index	1.376	1.336	1.336	n_L	1.336	–
Shift, mm	EC	EC	LS†	LS†	LS†	–
Tilt, °	EC	EC	LT†	LT†	LT†	–

EC, parameters derived from eigencorneas; LS, lens shift; LT, lens tilt.
* Anterior lens surface includes a phase correction to account for the noncorneal wavefront.
† Randomly generated based on values from the literature.[18,19]

Besides an aspherical surface, the anterior lens also includes a set of constant Zernike coefficients up to the fifth order ($Z_n^m[int]$; diameter, 5.50 mm) to account for the aberrations of noncorneal origins, which is equivalent to including a Zernike phase plate at the iris as both the anterior lens apex and the pupil lie in the same plane. These constant coefficients were determined by matching the wavefront calculated using the measured biometry of the original subjects with the measured wavefront.

Finally, as the crystalline lens tilt (LT_x, LT_y) and shift (LS_x, LS_y) could not be determined in the eye of the original subjects, these parameters are not included in the multivariate Gaussian model. Instead these are generated independently based on mean and standard deviation (SD) values found in the literature.[19,20]

Axial Length and Vitreous Depth. The Lenstar measures the ocular axial length from the corneal vertex until the retinal pigment epithelium, after which a fixed value of 0.200 mm is subtracted to bring it back to the inner limiting membrane in accordance with ultrasound measurements. Because the retinal image should be sharp on the photoreceptor layer rather than the internal limiting membrane, we followed the recent suggestion of Li et al.[21] to add a fixed value for retinal thickness *RT* of 0.200 mm to the measured axial length *L* prior to any calculations. Vitreous depth *V* is then calculated as $V = L - T - ACD - CCT - RT$.

Multivariate Gaussian Model

Based on the considerations above, the model consists of 12 eigencorneas, anterior chamber depth *ACD*, axial length *L*, lens power P_L, anterior lens radius r_{La}, posterior lens radius r_{Lp}, and lens thickness *T*. These parameters form an 18-dimensional point cloud that may be fitted with a linear combination of multivariate Gaussian functions,[5] which forms the core of the stochastic model. The fit was performed in Matlab 2011b (The Mathworks, Natick, MA, USA) using an expectation-maximization (EM) algorithm using the procedures described in References 5 and 11. Early trials indicated that a fit of two multivariate Gaussians gave a good fit accuracy, which could not be improved significantly by increasing the number of Gaussians.

Once a reliable fit is obtained, the Matlab program can use it to generate an unlimited number of random data points with a distribution that is very close to that of the original data. After conversion from eigencorneas to corneal Zernike coefficients, and determining the equivalent refractive index of the lens, these synthetic data points (or SyntEyes) may be used for further calculations. In this work, the model output is inserted into a custom Matlab ray tracing module to confirm the validity of the synthetic data with respect to the measured refraction and wavefront data. The refraction of the SyntEyes was calculated using the equations by Salmon and Thibos.[22] During the development of both the ray tracing module and the statistical model, the ray tracing results were verified against results obtained with commercial software (Zemax, Zemax LLC, Kirkland, WA, USA) to ensure compatibility.

For the reader's convenience, the Matlab program, along with a sample output file containing 1000 SyntEyes generated by the model, is provided as Supplementary Material B and C.

Statistics

The statistics in this work are mostly aimed at demonstrating the equality of the distributions of the original and the synthetic data. For this purpose, the two one-sided *t*-test (TOST) is used, which defines certain thresholds of equivalence between which the average of both sets may be considered equal.[23,24] Although some of the parameters involved may not be normally distributed, one can still use parametric testing such as *t*-tests, provided the populations involved are sufficiently large. Lumley et al.[25] stated that in most cases this threshold lies below 100 cases for a mild degree on nonnormality and below 500 for extremely high nonnormality. Given that the worst distributions in this work are only moderately nonnormal (as verified with Kolmogorov-Smirnov tests), this approach is warranted by the standards set by Lumley et al. All tests are performed at a confidence level of 0.05, adjusted with a Bonferroni correction in case of multiple simultaneous comparisons (indicated by 0.05/N, with N the number of comparisons performed).

Results

Verification of the Methods Used

Before the data produced by the proposed model may be considered as equivalent to the originally measured data, all aspects of this claim must be rigorously verified. One such aspect is the performance of the ray tracing module and eigencornea compression to reproduce the measured refraction and wavefront of the subjects based on their biometry. For spherical equivalent (Fig. 1a) and J_{45} (Fig. 1c), the histogram shows a very good match with those of the autorefractometer and wavefront measurements, whereas for J_0 (Fig. 1b), the distributions were a bit flatter, with a slightly higher occurrence of with-the-rule astigmatism in the calculated wavefronts compared with the measured wavefronts. The average Zernike

Investigative Ophthalmology & Visual Science

Downloaded From: http://iovs.arvojournals.org/pdfaccess.ashx?url=/data/Journals/IOVS/934916/ on 05/17/2016

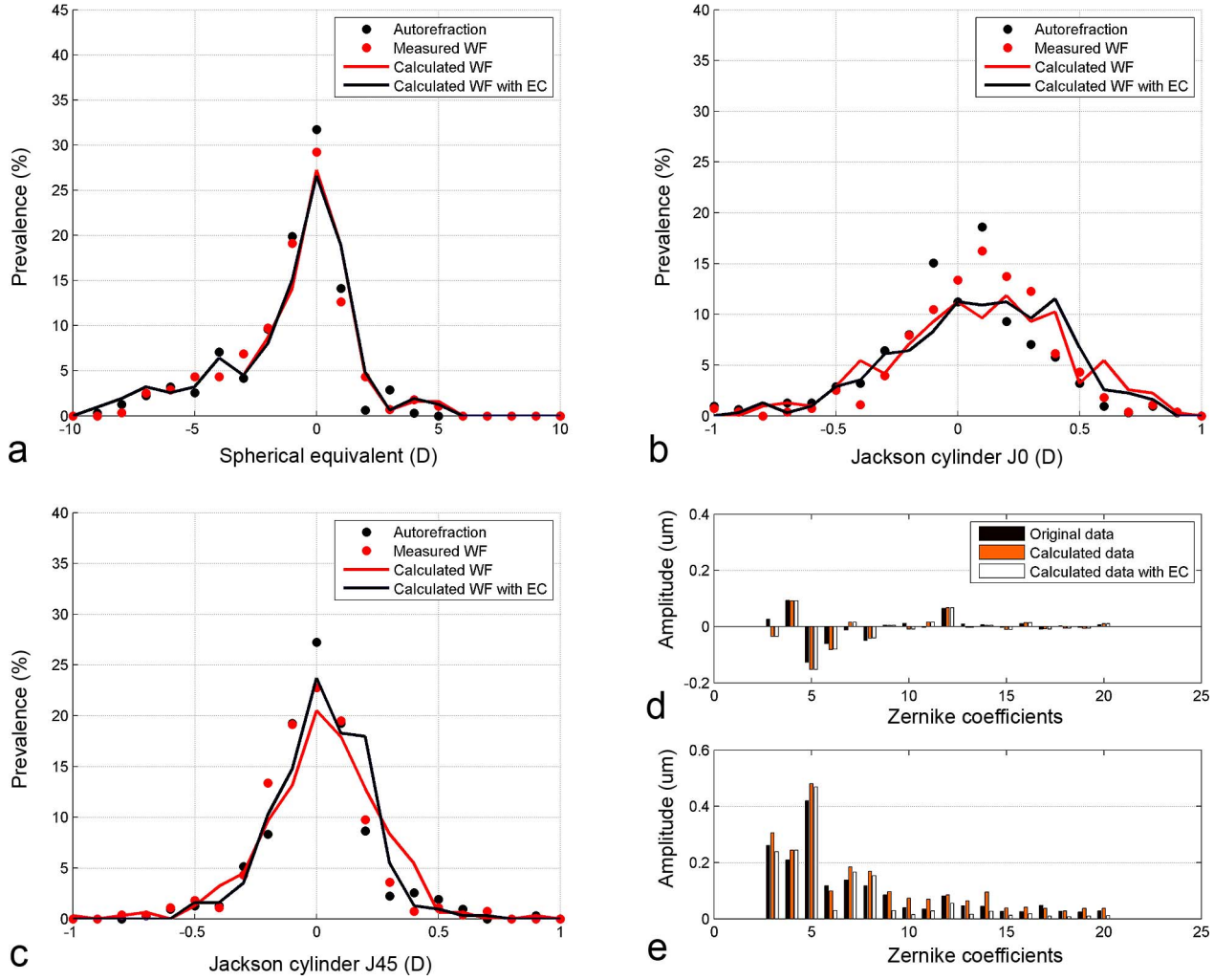

Figure 1. Verification of the refractive and wavefront results provided by the ray tracing module applied to the actual corneal elevation and after eigencornea (EC) compression for (**a**) spherical equivalent, (**b**) Jackson cylinder J_0, (**c**) Jackson cylinder J_{45}, (**d**) average, and (**e**) SD of the Zernike coefficients (eighth order, ∅ 5 mm; only first 20 coefficients are shown; mean and SD of Z_2^0 [nr 5] divided by 10 for better visualization).

coefficients presented in Figure 1d are all significantly equal to each other (TOST, $P > 0.05/45$, Bonferroni correction for 45 repeated comparisons), but in many of their SDs, significant differences are seen (*F*-test, $P < 0.05/45$; Fig. 1e). For the wavefront calculated based on the full corneal elevation, the SD is often significantly larger than that of the measured wavefront, whereas for the eigencornea compressed data, the SD is often significantly smaller (*F*-test, $P < 0.05/45$). Only for the second-order aberrations were the SDs similar to those of the measured wavefronts. Although this variability could be improved by including more than 12 eigencorneas, such a measure would also increase the dimensionality of the model, thus increasing the risk of overfitting the original data. We therefore opted to accept this as a limitation of the proposed model. More information on how well different numbers of eigencorneas reproduce the variability of the original wavefront can be found in Supplementary Material A.

Verification of the SyntEyes

All 18 parameters used by the statistical model are normally distributed within the 312 eyes of the original data (Kolmogorov-Smirnov test, $P > 0.05/109$; Table 3). Using the statistical eye model to generate 1000 SyntEyes and comparing their mean parameter values to those of the original data, both are significantly equal (TOST, $P > 0.05/109$). For the SD of the 18 parameters used by the eye model, no significant differences are seen between SyntEyes and the original data (*F*-test $P > 0.05/109$), but for most corneal Zernike coefficients Z_n^m (*CA*) and Z_n^m (*CP*), the SDs are significantly lower than those of the original data ($P < 0.05/109$). This is most likely the result of the eigencornea compression. A complete version of Table 3 is available in Supplementary Material D.

The distribution of the ocular surface positions of the SyntEyes also agrees well with those of the original data (Fig. 2).

Note that very similar results are found if a smaller group of 312 SyntEyes (i.e., the same number of eyes as the original data) is used, suggesting an invariance of the distribution against the number of generated SyntEyes.

In most cases, the Zernike coefficients of the wavefront and the autorefraction of the original data are nonnormal (Kolmogorov-Smirnov test, $P < 0.05/48$; Table 4). Often this is due to the presence of several outliers, but for *SE*, Z_0^0 (*WF*), and Z_2^0 (*WF*), the distributions were obviously leptokurtic and skewed (Fig. 3). Based on the criteria by Lumley et al.,[25] our population size is sufficiently large for parametric statistics, however, so the TOST and *F*-test could be performed for these parameters.

Investigative Ophthalmology & Visual Science

Downloaded From: http://iovs.arvojournals.org/pdfaccess.ashx?url=/data/Journals/IOVS/934916/ on 05/17/2016

Table 3. Comparison of the Biometry of the SyntEyes (1000 Eyes) With the Biometry of the Original Data (312 Eyes)

Parameter	Unit	KS*	Average (SD)		TOST†	*F*-Test*
			Original Data	SyntEyes		
EC_0	µm	0.985	348.79 (31.69)	348.07 (31.86)	Pass	0.921
EC_1	µm	0.653	−0.89 (22.19)	0.03 (22.23)	Pass	0.978
EC_2	µm	0.546	0.59 (10.09)	0.32 (10.04)	Pass	0.899
EC_3	µm	0.420	−0.22 (6.93)	−0.41 (6.88)	Pass	0.899
EC_4	µm	0.768	204.18 (4.55)	204.21 (4.48)	Pass	0.802
EC_5	µm	0.835	−2.10 (4.31)	−1.98 (4.38)	Pass	0.727
EC_6	µm	0.937	−0.05 (2.95)	−0.11 (2.93)	Pass	0.854
EC_7	µm	0.710	−0.26 (2.73)	−0.13 (2.66)	Pass	0.639
EC_8	µm	0.939	0.25 (2.12)	0.25 (2.05)	Pass	0.605
EC_9	µm	0.128	0.04 (1.78)	0.04 (1.81)	Pass	0.665
EC_{10}	µm	0.961	−0.01 (1.31)	−0.06 (1.33)	Pass	0.778
EC_{11}	µm	0.005	0.04 (1.18)	0.00 (1.16)	Pass	0.713
ACD	mm	0.701	2.89 (0.39)	2.90 (0.39)	Pass	0.965
T	mm	0.066	4.06 (0.38)	4.06 (0.38)	Pass	0.830
L	mm	0.338	24.04 (1.11)	24.04 (1.08)	Pass	0.629
r_{La}	mm	0.544	10.38 (1.21)	10.54 (1.19)	Pass	0.823
r_{Lp}	mm	0.547	−6.84 (0.76)	−6.94 (0.75)	Pass	0.826
P_L	D	0.516	23.39 (2.05)	22.55 (1.97)	Pass	0.756
CCT‡	µm	0.989	549.09 (31.29)	548.39 (31.46)	Pass	0.919
Z_n^m (*CA*)‡	µm	**2/45§**			0/45§	**38/45§**
Z_n^m (*CP*)‡	µm	0/45§			0/45§	**35/45§**

KS, Kolmogorov-Smirnov test for normality.
* $P < 0.05/109 = 4.59 \times 10^{-4}$ (Bonferroni correction) indicates a significant difference (in bold).
† $P > 0.05/109 = 4.59 \times 10^{-4}$ (Bonferroni correction) indicates a significant equality (in bold).
‡ Derived from eigencorneas $EC_0,\ldots,EC_{11}$.
§ Number of comparisons with a significant difference.

Both the calculated refraction and the calculated wavefront are significantly equal to the measured values of the original data (TOST, $P > 0.05/48$; Table 4), but the SDs of the SyntEyes is in most cases significantly smaller than that of the original data (*F*-test, $P < 0.05/48$). This is also illustrated in Figure 3, where the histograms of the calculated Zernike coefficients up to the fourth order are shown for 1000 SyntEyes (black lines) and compared with the measured wavefronts of the original data (gray bars). Overall, the agreement between both is good, except for the trefoil coefficients ($Z_3^{\pm 3}$), where the SyntEyes display considerably less variation compared with the original data. To a lesser degree, this is also seen for Z_4^{-4} and Z_4^{+2}. A complete version of Table 4, as well as a comparison of the wavefront metrics proposed by Marsack et al.,[26] is available in Supplementary Material D.

The correlation coefficients between the parameters of the SyntEyes are close to those of the corresponding parameters of the original data for the intraocular distances, eigencorneas, and the Zernike elevation coefficients of piston (Z_0^0), tilt ($Z_1^{\pm 1}$), defocus (Z_2^0), astigmatism ($Z_2^{\pm 2}$), coma ($Z_3^{\pm 1}$), and spherical aberration (Z_4^0). For the other third- and fourth-order Zernike coefficients, the correlations between the SyntEyes parameters were higher than between the parameters of the

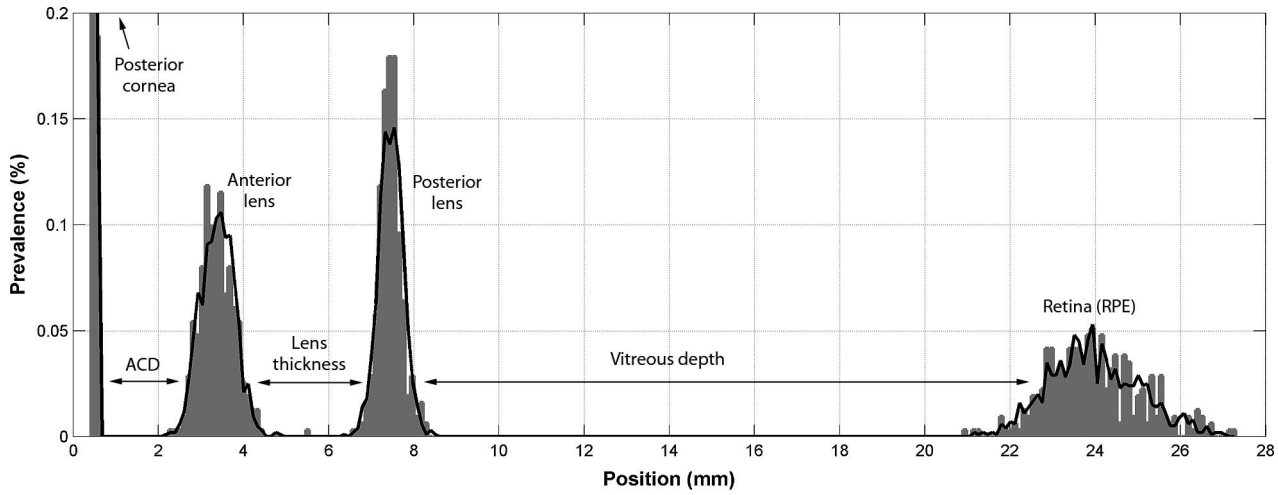

Figure 2. Combined histogram showing the positions of the ocular surfaces in the original data (*gray bars*) and the SyntEyes (*black line*).

Investigative Ophthalmology & Visual Science

Downloaded From: http://iovs.arvojournals.org/pdfaccess.ashx?url=/data/Journals/IOVS/934916/ on 05/17/2016

Table 4. Comparison of the Calculated Refraction and Wavefront for 1000 SyntEyes With the Measured Values for the Original Data (312 Eyes)

			Average (SD)			
Parameter	**Unit**	**KS***	**Original Data**	**SyntEyes**	**TOST†**	***F*-Test***
SE	D	**<0.001**	−1.23 (2.29)	−1.04 (2.68)	Pass	0.001
J_0	D	0.018	0.01 (0.35)	0.07 (0.38)	Pass	0.152
J_{45}	D	0.019	0.00 (0.21)	0.00 (0.18)	Pass	**<0.001**
Z_n^m (*WF*)	μm	**22/45‡**			0/45‡	**40/45‡**

Wavefront measurements available for 277 eyes. KS, Kolmogorov-Smirnov test for normality.
* $P < 0.05/48 = 1.042 \times 10^{-3}$ (Bonferroni correction) indicates a significant difference (in bold).
† $P > 0.05/48 = 1.042 \times 10^{-3}$ (Bonferroni correction) indicates a significant equality (in bold).
‡ Number of comparisons with a significant difference.

original data, associated with the SyntEyes' lower degree of randomness (Fig. 4).

Potential Applications of SyntEyes

One of the anticipated applications of SyntEyes is the assessment of intraocular lens (IOL) design and IOL power formulas in eyes with a large variety of biometry. This is illustrated in Figure 5, showing the estimated refractive outcomes for the same 1000 SyntEyes as before implanted with a Morcher 89a "Bag in the Lens" IOL.[27] As this IOL has a 0% rate for posterior capsular opacification[27] and a very high degree of postoperative centration and rotation stability,[28,29] it is an ideal lens to verify the optical performance of the SyntEyes with clinical data. All lens powers were calculated using the Sanders-Retzlaff-Kraff/Theoretical (SRK/T) formula,[30] aiming at postoperative emmetropia. Information on the radii

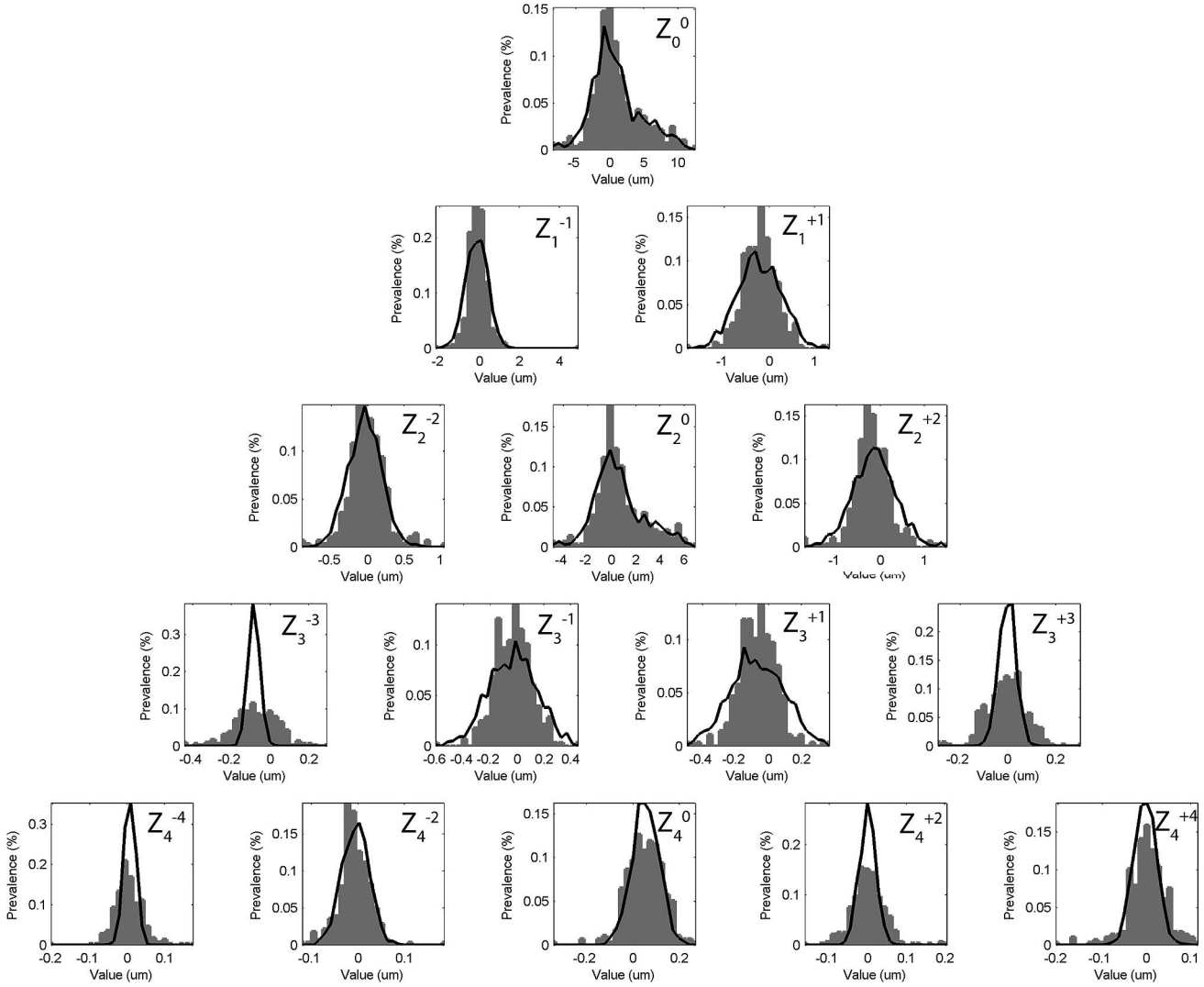

Figure 3. Histogram of the Zernike coefficients up to the fourth order for the original data (277 eyes; *gray bars*) and 1000 SyntEyes (*black lines*).

Investigative Ophthalmology & Visual Science

Downloaded From: http://iovs.arvojournals.org/pdfaccess.ashx?url=/data/Journals/IOVS/934916/ on 05/17/2016

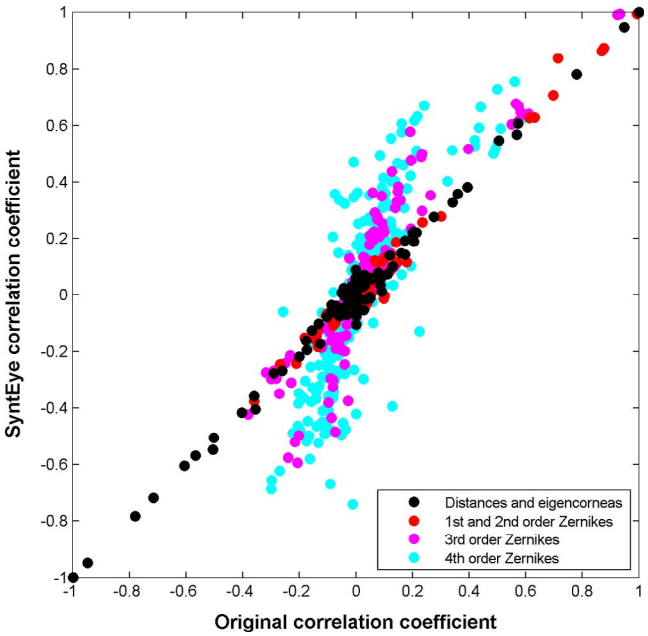

FIGURE 4. Correlation coefficients of the SyntEyes compared with those of the original data for the intraocular distances, eigencorneas, and elevation Zernike coefficients of both corneal surfaces.

of curvature and lens thickness were obtained directly from the manufacturer (Morcher GmbH, Stuttgart, Germany).

These estimated outcome results are compared with the refraction data of 320 eyes implanted with the Bag in the Lens (320 patients; male/female: 42.2%/57.8%; age: 69.5 ± 10.8 years; postoperative date: 10.1 ± 7.2 months; no ocular comorbidities) taken from Reference 27. As these are subjective refraction data, recorded at least 5 weeks postoperatively, the patient's pupil diameter at the time of measurement is unknown. The refraction for the SyntEyes is therefore calculated for a pupil diameter of 3, 4, and 5 mm and then averaged over the three. As is seen in Figure 5, the resulting distribution of the refraction in SyntEyes is very close to that measured in the pseudophakic eyes. Moreover, the spherical aberration Z_4^0 (*WF*) of the pseudophakic SyntEyes lies close to 0.20 µm, which is in the range of the values reported in the literature for spherical IOLs.

Similarly the model can be used to assess the outcome of laser refractive surgery by applying a virtual laser correction to the SyntEyes' anterior corneal surface. For this purpose, the outcome of the SyntEye model was compared with pre- and postoperative wavefront data taken from 71 myopic eyes that underwent laser epithelial keratomileusis (LASEK) collected in a previous study[31] (37 patients; male/female: 29.7%/70.3%; age: 33.6 ± 9.4 years; postoperative date: 6.2 ± 4.5 months; no ocular comorbidities; no cylinder correction >1 D). These eyes were treated with an InPro GAUSS laser system (InPro GmbH, Norderstedt, Germany), which delivers a broad Gaussian laser beam with a diameter of 6.5 mm. This process can be simulated by removing a similar profile from the anterior cornea for all 365 SyntEyes with a myopia higher than −1 D (taken from the same set of SyntEyes as before). The amount of ablation required for emmetropia was determined using the Munnerlyn algorithm for myopia.[32] Assuming perfect centration and a perfect beam profile, the postrefractive *SE* of the SyntEyes is similar to what is found in the real post-LASEK eyes (Fig. 6a), albeit with a sharper distribution. The Zernike coefficients of both the pre- and postoperative wavefronts are similar for both the real eyes and the SyntEyes (Figs. 6b, 6c), apart from the preoperative astigmatism (Z_2^{+2}), which is higher in the real eyes and two postoperative third-order coefficients (Z_3^{-3}, Z_3^{-1}) that are more pronounced in the real eyes as well. As before, the variability of the Zernike coefficients is higher in the real eyes that in the SyntEyes (not shown). The SyntEyes data for this example are included in Supplementary Material C.

DISCUSSION

The SyntEyes model presents a means to produce an unlimited amount of synthetic biometric data, with mean values that are statistically indistinguishable from the original data it is based on. The variability of the most important biometric parameters (i.e., the curvatures of the optical interfaces and the intraocular distances) lies close to that of the original data, whereas for the higher-order Zernike coefficients, the variations of the SyntEyes are generally lower due to the eigencorneas. Overall, this translates into a very powerful tool for researchers in physiological optics and for simulations of cataract and refractive treatments, as is demonstrated by the examples above.

The SyntEyes model has the distinct advantages that it provides the biological variability that is missing from the classic, generic eye models and that it can be easily implemented in ray tracing software for batch processing. This means that the model has many potential applications, such as the standardization of new IOL designs, including tolerance analysis, or comparison of IOL power formulas over a data set with a large biometric variation, rather than on a fixed generic eye model. Helpful suggestions on how to set up such

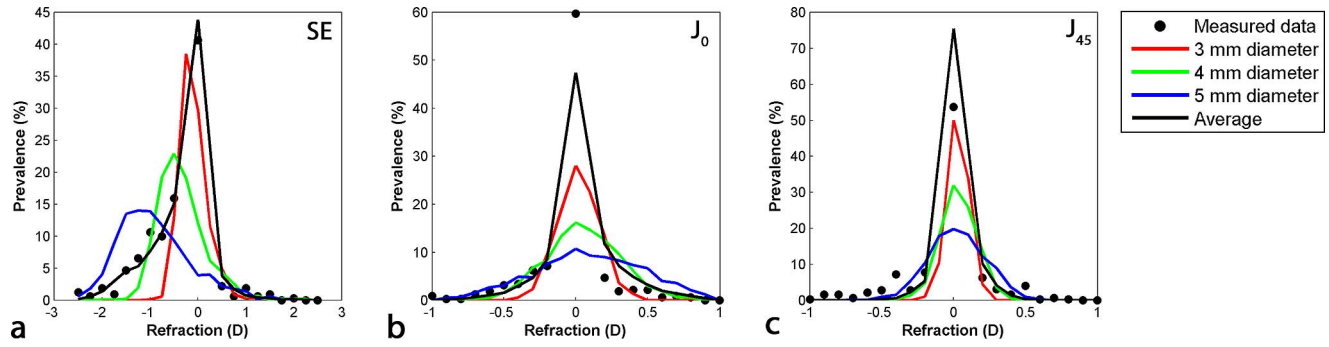

FIGURE 5. Distribution of the estimated refraction of 1000 SyntEyes implanted with a Morcher 89a "Bag in the Lens" IOL targeting emmetropia for three pupil diameters compared with previously measured data of 320 pseudophakic eyes. The central three bins (–0.25, 0, and 0.25 D) are combined for both the measured and the average SyntEyes data. (**a**) Spherical equivalent, (**b**) Jackson cylinder J_0, and (**c**) Jackson cylinder J_{45}.

Investigative Ophthalmology & Visual Science

Downloaded From: http://iovs.arvojournals.org/pdfaccess.ashx?url=/data/Journals/IOVS/934916/ on 05/17/2016

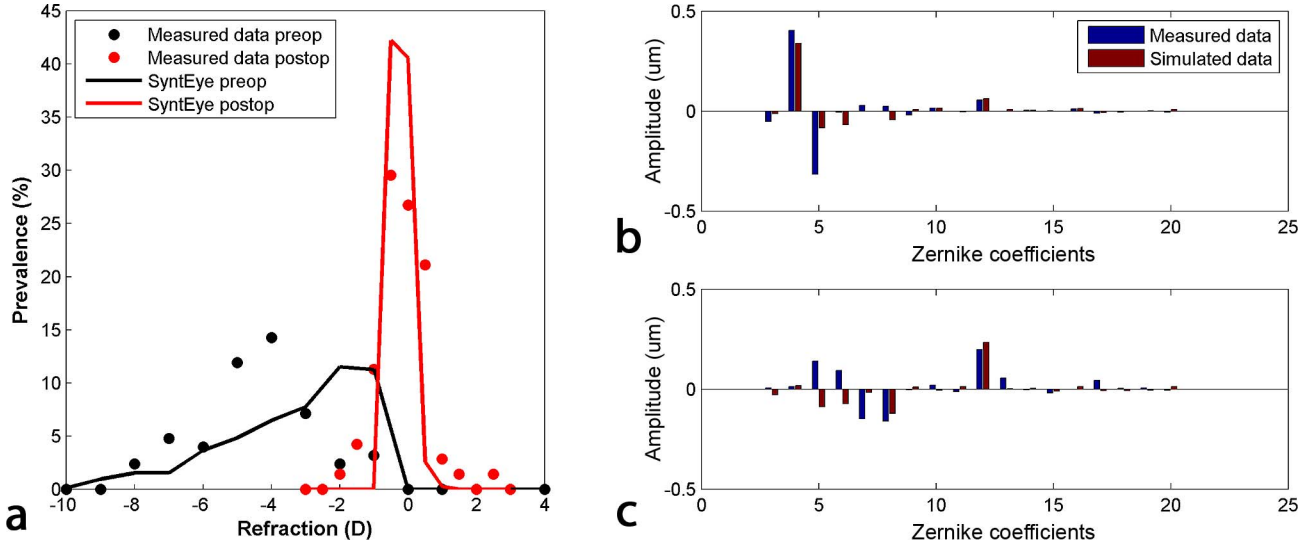

FIGURE 6. Distribution of the estimated SE refraction of 365 myopic SyntEyes before and after they underwent refractive laser correction with a broad Gaussian beam compared with the outcome of 71 real myopic eyes of 37 patients before and after LASEK. (**a**) Distribution of SE, (**b**) preoperative Zernike coefficients, and (**c**) postoperative Zernike coefficients (mean of Z_2^0 [nr 5] divided by 10 for better visualization).

studies may be found in the protocols recently proposed by Hoffer et al.[33] Similarly, the effects of laser refractive surgery can be simulated for a wide variety of biometry values, which could potentially improve the postoperative outcome. Alternatively, one could simulate how the IOL power should be calculated in postrefractive patients to identify combinations of biometric parameters for which a surgical procedure could lead to previously unexpected outcomes. Finally, the SyntEyes model may be useful for governments or regulatory authorities (e.g., Food and Drug Administration and European Medicines Agency) to refine the indications for reimbursement of certain therapies or improve laser safety thresholds.[34,35]

Provided sufficient appropriate data are available, similar models may also be built for other healthy or pathological populations. This could for example be done for eyes of young children, non-Caucasian subjects, or subjects in nonindustrialized regions where the prevalence of myopia is relatively low. Other possible extensions could be the inclusion of ocular aging,[36–39] wide angle refraction,[2,3,40–44] a gradient index lens,[4,36,44,45] accommodation,[1,2,36,46,47] or corneal biomechanics.[48]

However, the model also has several inherent limitations that one must keep in mind, mostly associated with the fact it takes its properties from the original data it is based on and is therefore unable to increase the information content. Furthermore, the use of the eigencornea compression reduces the variability and the correlation coefficients of the higher-order corneal Zernike coefficients and, consequently, those of the higher-order wavefront aberrations as well. However, the validations with the original, the pseudophakic, and the postrefractive data demonstrated that the variability of the refraction and the most important Zernike coefficients in the SyntEyes does not deviate too far from those found in the measured data. We are therefore confident that this reduced higher-order variability will not hamper the performance of the model by any noticeable degree.

Finally, another limitation of the model is the fact that the lens parameters were not measured, but estimated using multiple linear regressions. Even though these regressions perform quite satisfactorily in the description of lens curvatures in a population, they may still produce values that deviate substantially from their actual amounts.[16] Given the stochastic nature of the SyntEyes model, which only requires the mean and covariance values in order to produce plausible estimates for the lens curvatures values, these parameters are probably well integrated into the model. Nevertheless, once phakometry equipment becomes available clinically, for example, based on the crystalline lens topography,[49] we will consider updating the current model with these parameters to keep the current model relevant.

Acknowledgments

The authors thank Sien Jongenelen, Irene Ruiz, Nadia Zakaria, Jeroen Claeys, and Greet Vandeweyer for support in collecting the data and Kristien Wouters for assistance with the statistics.

Supported by research grants from the Flemish government agency for Innovation by Science and Technology (Grant IWT/110684) and the Spanish Ministry of Economy and Competitiveness (FIS2014-58303-P).

Disclosure: **J.J. Rozema**, None; **P. Rodriguez**, None; **R. Navarro**, None; **M.-J. Tassignon**, None

References

1. Gullstrand A. Appendix II and IV. In: von Helmholtz H, ed. *Handbuch der Physiologischen Optik*. 3rd ed. Hamburg, Germany: Voss; 1909;301–358, 382–415.
2. Navarro R, Santamaría J, Bescós J. Accommodation-dependent model of the human eye with aspherics. *J Opt Soc Am A*. 1985; 2:1273–1280.
3. Escudero-Sanz I, Navarro R. Off-axis aberrations of a wide-angle schematic eye model. *J Opt Soc Am A*. 1999;16:1881–1891.
4. Liou H-L, Brennan NA. Anatomically accurate, finite model eye for optical modeling. *J Opt Soc Am A*. 1997;14:1684–1695.
5. Rozema JJ, Tassignon M-J. The Bigaussian nature of ocular biometry. *Optom Vis Sci*. 2014;91:713–722.
6. Guo H, Wang Z, Zhao Q, Quan W, Wang Y. Individual eye model based on wavefront aberration. *Optik*. 2005;116:80–85.
7. Ortiz D, Anera R, Saiz J, et al. Corneal changes induced by laser ablation: study of the visual-quality evolution by a customized eye model. *J Modern Opt*. 2006;53:1605–1618.

Downloaded From: http://iovs.arvojournals.org/pdfaccess.ashx?url=/data/Journals/IOVS/934916/ on 05/17/2016

8. Rosales P, Marcos S. Customized computer models of eyes with intraocular lenses. *Opt Express*. 2007;15:2204–2218.
9. Navarro R, González L, Hernández-Matamoros JL. On the prediction of optical aberrations by personalized eye models. *Optom Vis Sci*. 2006;83:371–381.
10. Canovas C, Artal P. Customized eye models for determining optimized intraocular lenses power. *Biomed Opt Express*. 2011;2:1649–1662.
11. Rozema JJ, Atchison DA, Tassignon M-J. Statistical eye model for normal eyes. *Invest Ophthalmol Vis Sci*. 2011;52:4525–4533.
12. Sorsby A, Benjamin B, Bennett AG. Steiger on refraction: a reappraisal. *Br J Ophthalmol*. 1981;65:805–811.
13. Thibos LN, Hong X, Bradley A, Cheng X. Statistical variation of aberration structure and image quality in a normal population of healthy eyes. *JOSA A*. 2002;19:2329–2348.
14. Zhao H. Optical ensemble analysis of intraocular lens performance through a simulated clinical trial with ZEMAX. *Optics Lett*. 2009;34:7–9.
15. Rodríguez P, Navarro R, Rozema JJ. Eigencorneas: application of principal component analysis to corneal topography. *Ophthalmic Physiol Opt*. 2014;34:667–677.
16. Rozema JJ, Atchison DA, Kasthurirangan S, Pope JM, Tassignon M-J. Methods to estimate the size and shape of the unaccommodated crystalline lens in vivo. *Invest Ophthalmol Vis Sci*. 2012;53:2533–2540.
17. Rozema JJ, Atchison DA, Tassignon M-J. Comparing methods to estimate the human lens power. *Invest Ophthalmol Vis Sci*. 2011;52:7937–7942.
18. Berrio E, Tabernero J, Artal P. Optical aberrations and alignment of the eye with age. *J Vis*. 2010;10(14):34.
19. Chang Y, Wu H-M, Lin Y-F. The axial misalignment between ocular lens and cornea observed by MRI (I)—at fixed accommodative state. *Vis Res*. 2007;47:71–84.
20. Bennett A. A method of determining the equivalent powers of the eye and its crystalline lens without resort to phakometry. *Ophthal Physiol Optics*. 1988;8:53–59.
21. Li S-M, Wang N, Zhou Y, et al. Paraxial schematic eye models for 7- and 14-year-old Chinese children: paraxial schematic eyes for Chinese children. *Invest Ophthalmol Vis Sci*. 2015;56:3577–3583.
22. Salmon TO, Thibos LN. Videokeratoscope–line-of-sight misalignment and its effect on measurements of corneal and internal ocular aberrations. *JOSA A*. 2002;19:657–669.
23. Westlake WJ. Symmetrical confidence intervals for bioequivalence trials. *Biometrics*. 1976;9:741–744.
24. Schuirmann DJ. A comparison of the two one-sided tests procedure and the power approach for assessing the equivalence of average bioavailability. *J Pharmacokinet Biop*. 1987;15:657–680.
25. Lumley T, Diehr P, Emerson S, Chen L. The importance of the normality assumption in large public health data sets. *Ann Rev Publ Health*. 2002;23:151–169.
26. Marsack JD, Thibos LN, Applegate RA. Metrics of optical quality derived from wave aberrations predict visual performance. *J Vis*. 2004;4(4):328.
27. Tassignon M-J, Gobin L, Mathysen D, Van Looveren J, De Groot V. Clinical outcomes of cataract surgery after bag-in-the-lens intraocular lens implantation following ISO standard 11979-7: 2006. *J Cataract Refract Surg*. 2011;37:2120–2129.
28. Verbruggen KH, Rozema JJ, Gobin L, Coeckelbergh T, De Groot V, Tassignon M-J. Intraocular lens centration and visual outcomes after bag-in-the-lens implantation. *J Cataract Refract Surg*. 2007;33:1267–1272.
29. Rozema JJ, Gobin L, Verbruggen K, Tassignon M-J. Changes in rotation after implantation of a bag-in-the-lens intraocular lens. *J Cataract Refract Surg*. 2009;35:1385–1388.
30. Retzlaff JA, Sanders DR, Kraff MC. Development of the SRK/T intraocular lens implant power calculation formula. *J Cataract Refract Surg*. 1990;16:333–340. (Erratum: *J Cataract Refract Surg*. 1990;16:528).
31. Rozema JJ, Coeckelbergh T, Van den Berg T, et al. Straylight before and after LASEK in myopia: changes in retinal straylight. *Invest Ophthalmol Vis Sci*. 2010;51:2800–2804.
32. Munnerlyn CR, Koons SJ, Marshall J. Photorefractive keratectomy: a technique for laser refractive surgery. *J Cataract Refract Surg*. 1988;14:46–52.
33. Hoffer KJ, Aramberri J, Haigis W, et al. Protocols for studies of intraocular lens formula accuracy. *Am J Ophthalmol*. 2015;160:403–405.
34. Wooddell DA Jr. *Probabilistic Model for Laser Damage to the Human Retina*. Wright-Patterson AFB, OH: 2012.
35. Wooddell DA, Schubert-Kabban CM, Hill RR. Analysis of the influences of biological variance, measurement error, and uncertainty on retinal photothermal damage threshold studies. *SPIE BiOS*. 2012:822114–822116.
36. Navarro R. Adaptive model of the aging emmetropic eye and its changes with accommodation. *J Vis*. 2014;14(13):21.
37. Atchison DA, Markwell EL, Kasthurirangan S, Pope JM, Smith G, Swann PG. Age-related changes in optical and biometric characteristics of emmetropic eyes. *J Vis*. 2008;8(4):29.
38. Smith G, Atchison DA, Pierscionek BK. Modeling the power of the aging human eye. *JOSA A*. 1992;9:2111–2117.
39. Koretz JF, Kaufman PL, Neider MW, Goeckner PA. Accommodation and presbyopia in the human eye—aging of the anterior segment. *Vision Res*. 1989;29:1685–1692.
40. Kooijman AC. Light distribution on the retina of a wide-angle theoretical eye. *JOSA A*. 1983;73:1544–1550.
41. Pomerantzeff O, Pankratov M, Wang G, Dufault P. Wide-angle optical model of the eye. *Am J Optometry Physiol Optics*. 1984;61:166–176.
42. Drasdo N, Fowler C. Non-linear projection of the retinal image in a wide-angle schematic eye. *Br J Ophthalmol*. 1974;58:709–714.
43. Atchison DA. Optical models for human myopic eyes. *Vision Res*. 2006;46:2236–2250.
44. Goncharov AV, Dainty C. Wide-field schematic eye models with gradient-index lens. *JOSA A*. 2007;24:2157–2174.
45. Siedlecki D, Kasprzak H, Pierscionek BK. Schematic eye with a gradient-index lens and aspheric surfaces. *Optics Lett*. 2004;29:1197–1199.
46. Popiolek-Masajada A, Kasprzak H. Model of the optical system of the human eye during accommodation. *Ophthalmic Physiol Optics*. 2002;22:201–208.
47. Popiolek-Masajada A, Kasprzak HT. A new schematic eye model incorporating accommodation. *Optometry Vision Sci*. 1999;76:720–727.
48. Roy AS, Dupps WJ. Patient-specific modeling of corneal refractive surgery outcomes and inverse estimation of elastic property changes. *J Biomechan Engin*. 2011;133:011002.
49. Sun M, Birkenfeld J, de Castro A, Ortiz S, Marcos SOCT. 3-D surface topography of isolated human crystalline lenses. *Biomed Opt Express*. 2014;5:3547–3561.

Investigative Ophthalmology & Visual Science

Downloaded From: http://iovs.arvojournals.org/pdfaccess.ashx?url=/data/Journals/IOVS/934916/ on 05/17/2016